Tetragonal MnO_2 Nanoparticles Synthesized via Lagerstroemia speciosa: Structural Characterization and Photocatalytic Potential

Jagdish Arekar
North Maharashtra University
Dipak. J. Garole
Government of Maharashtra
Yogesh R. Toda
yogeshtoda@gmail.com

Government College of Engineering
Ratnamala S. Bendre
North Maharashtra University

Research Article

Keywords: MnO_2-NPs, green synthesis, Lagerstroemia speciosa, photo catalysis, UV–Vis–IR, XRD, FESEM, dye degradation

Posted Date: June 3rd, 2025

DOI: https://doi.org/10.21203/rs.3.rs-6715891/v1

Additional Declarations: No competing interests reported.

Abstract

Manganese oxide nanoparticles (MnO_2-NPs) were biosynthesized using an aqueous extract of *Lagerstroemia speciosa* leaf powder. The plant is rich in phytochemicals such as phenolic compounds, alkaloids, α-amino acids, steroids, organic acids, terpenoids, reducing sugars, glycosides, carbohydrates, saponins, starch, flavonoids, and tannins. The phenolic compounds acted as both reducing and capping agents. The synthesized nanoparticles were characterized using UV–Vis–IR spectroscopy, X-ray diffraction (XRD), field emission scanning electron microscopy (FESEM), thermogravimetric analysis (TGA), differential scanning calorimetry (DSC), and Fourier-transform infrared spectroscopy (FTIR). The UV–Vis–IR spectrum revealed a distinct absorption peak at 365 nm, confirming the formation of MnO_2-NPs. FESEM images indicated rough, spherical, randomly oriented particles with sizes ranging from 83–400 nm. XRD analysis confirmed a pure tetragonal structure with preferential (110) plane orientation. The photocatalytic performance of the MnO_2-NPs was assessed via the sunlight-driven decolourization of methyl orange (MO) and bromocresol green (BCG) dyes.

1. Introduction

In nanotechnology, particle size plays a crucial role in determining the material's properties. Nanoparticles exhibit unique structural, magnetic, and optical behaviours, governed by their size, shape, morphology, and composition [1]. Morphology and dimension are particularly important, as they contribute to the stability and functionality of nanoparticles [2, 3]. Due to their high specific surface area and distinct electronic, chemical, and physical properties, metal nanoparticles especially manganese oxide nanoparticles—have broad applications in batteries, catalysts, water treatment, molecular sieves, optoelectronics, and magnetic materials [4, 5].

Manganese oxide nanoparticles (MnO_2-NPs) are also being explored for solar cell applications due to their promising electronic and optical properties [6]. These nanoparticles can be synthesized via several techniques, including femtosecond laser ablation [7], reflux treatment [8], redox reaction [9], green synthesis [10], co-precipitation [11], and sol–gel methods [12].

Among these, green synthesis has gained attention as a sustainable, eco-friendly approach. This method utilizes plant parts leaves, stems, roots, bark, seeds or microbial agents like fungi, yeast, and bacteria. The metal ions are reduced by natural biomolecules such as flavonoids, tannins, saponins, terpenoids, steroids, and alkaloids [13–15]. Manganese oxide nanoparticles are particularly attractive due to their cost-effectiveness, environmental compatibility, and potential in various applications including photo catalysis, biomedicine, sensing, and optoelectronics, owing to their surface reactivity and physicochemical characteristics.

Despite significant studies focusing on the electronic properties of MnO_2-NPs, their photocatalytic performance especially under sunlight has been less explored. This work investigates the green synthesis of MnO_2-NPs using *Lagerstroemia speciosa* leaf extract, with particular emphasis on their ability to decolorize methyl orange and bromocresol green dyes under solar irradiation.

2. Materials and Methods

2.1 Preparation of Plant Extract

Fresh, mature leaves of *Lagerstroemia speciosa* were collected, thoroughly washed with distilled water to remove dirt and impurities, and then air-dried. Five grams of the dried leaves were finely ground into powder and extracted with 100 mL of Milli-Q water by boiling the mixture in a water bath for 30 minutes. The extract was filtered through Whatman No. 1 filter paper to remove solid residues. The resulting aqueous extract was stored at 6°C until further use.

2.2 Synthesis of Manganese Oxide Nanoparticles (MnO_2-NPs)

Manganese acetate ($Mn(CH_3COO)_2$) was used as the precursor salt for nanoparticle synthesis. A 0.1 M solution was prepared by dissolving 1.73 g of manganese acetate in 100 mL of distilled water. The synthesis was carried out by adding 100 mL of *Lagerstroemia speciosa* leaf extract dropwise to the 100 mL of 0.1 M manganese acetate solution preheated to 60°C under continuous stirring. The mixture was then heated at 80°C for 30 minutes. The gradual colour change from colourless to dark brown or black indicated the formation of MnO_2 nanoparticles. After cooling to room temperature, the solution was centrifuged at 15,000 rpm for 15 minutes. The supernatant was discarded, and the collected nanoparticles were dried in an oven at 60°C for further characterization.

3. Materials Characterization

3.1 Structural Properties: X-ray Diffraction (XRD) Analysis

The structural properties of manganese oxide nanoparticles (MnO_2-NPs) were analysed using X-ray diffraction (XRD) on a Bruker D8 Advanced model (Germany) equipped with Cu $K\alpha_1$ radiation (λ = 1.54056 Å). Data were collected over a 2θ range of 20°–80° with a scanning speed of 0.5°/min. The detector used was a fast-counting silicon strip (Bruker Lynx Eye). XRD measurements were performed both before and after calcination. The uncalcined manganese oxide sample showed no discernible diffraction peaks. After calcination at 600°C for 2 hours, distinct peaks appeared at 2θ values of 28.74°, 37.46°, 41.28°, 42.30°, 47.35°, 57.60°, and 59.50°, corresponding to the (110), (101), (200), (111), (210), (211), and (220) lattice planes, respectively. The diffraction pattern confirmed a polycrystalline nature of the sample.

The XRD pattern was indexed to the tetragonal phase of manganese oxide, consistent with JCPDS card No. 24–0735, with lattice parameters a = b = 9.81 Å and c = 2.84 Å [17]. No additional peaks from impurities were observed, indicating high purity and crystallinity of the synthesized nanoparticles.

The average crystallite size was estimated using the Scherrer formula applied to the main diffraction peaks, yielding a size of approximately 25.3 nm [16].

3.2 Field Emission Scanning Electron Microscopy (FESEM)

Field emission scanning electron microscopy (FESEM) was employed to investigate the surface morphology and microstructure of the manganese oxide nanoparticles. FESEM images were obtained using a Hitachi S-4800 instrument (Hitachi High Technologies Corporation, Japan).

Figure 3 (a–c) presents FESEM images of manganese oxide nanoparticles calcined at 600°C, captured at different magnifications (100×, 20,000×, and 50,000×). The images reveal that the nanoparticles exhibit polymorphic morphology, with predominantly irregular, spherical, and randomly oriented particles formed via the *Lagerstroemia speciosa* leaf extract-mediated synthesis.

Particle aggregation is evident, which can be attributed to high surface energy, electrostatic interactions, and polarity effects [18]. Such aggregation may enhance adsorption properties, beneficial for dye removal applications, due to the increased surface area and reduced particle size [19]. Furthermore, the reduction in particle size can be credited to the capping effect of active organic compounds in the plant extract, which inhibit excessive particle growth [20]. The nanoparticles show a size distribution ranging from approximately 83 nm to 400 nm. The presence of voids among the particles suggests potential sites for doping or further functionalization to enhance structural and functional properties.

3.3 Fourier Transform Infrared Spectroscopy (FTIR)

Fourier transform infrared spectroscopy (FTIR) was used to identify the functional groups present in the manganese oxide nanoparticles and to understand the modes of vibration of chemical bonds within the nanocomposites. The FTIR spectrum of the MnO_2 nanoparticles was recorded in the range of 4000 – 400 cm^{-1}, as shown in Fig. 4.

A prominent absorption peak at 579 cm^{-1} corresponds to the Mn–O bond, indicating the Mn–O stretching vibration characteristic of the O–Mn–O framework in MnO_2 [21–23]. The absorption band at 1032 cm^{-1} is attributed to O–H bending vibrations coupled with Mn atoms, while the peak at 1416 cm^{-1} corresponds to the C–N stretching of amine groups. The peak observed near 1557 cm^{-1} is assigned to nitrate groups [24].

Additional absorption bands at 2324 cm^{-1}, 2829 cm^{-1}, 2943 cm^{-1}, and 3745 cm^{-1} correspond to the stretching vibrations of C–OH, C ≡ C, C–H, and –OH groups, respectively [25–27]. These functional groups likely originate from various phytochemicals in the *Lagerstroemia speciosa* leaf extract, such as flavonoids and alkaloids, which act as both reducing and capping agents during nanoparticle synthesis [28, 29].

3.4 Thermogravimetric Analysis (TGA/DTA)

Thermogravimetric analysis (TGA) and differential thermal analysis (DTA) were conducted to evaluate the thermal stability and decomposition behaviour of the synthesized manganese oxide nanoparticles.

The TGA/DTA curves are presented in Fig. 5 (a, b). The heating process was initiated at room temperature and increased to 850°C at a rate of 10°C/min under a nitrogen atmosphere.

The initial weight loss observed between 20°C and 100°C corresponds to the removal of physically adsorbed water and water of crystallization, indicating dehydration of the manganese oxide surface. A second minor mass loss was observed between 100°C and 260°C, which can be attributed to the release of unreacted organic molecules originating from the *Lagerstroemia speciosa* leaf extract used during the biosynthesis process.

A significant mass loss occurred between 300°C and 320°C, accounting for a total weight reduction of approximately 65–69%. This is likely due to the decomposition of organic compounds and partial crystallization processes. The sustained thermal stability observed beyond 550°C suggests the formation of stable manganese oxide phases, particularly α-MnO_2, characterized by enhanced ionic bonding and lattice ordering.

No appreciable weight loss was detected in the temperature range of 550–850°C, indicating that the MnO_2 nanoparticles exhibit high thermal stability and are resistant to further decomposition [30, 31].

The DTA curve shows a prominent endothermic peak around 455°C, which is attributed to the melting behavior associated with the nanocrystalline nature of the material. A broader peak at approximately 600°C is ascribed to a phase transition from α-MnO_2 to another polymorphic form of MnO_2.

$$Mn(CH_3COO)_2\,2H_2O \longrightarrow Mn_3O_4 + 4\,CO_2 + C_8H_{18} + 6H_2O\uparrow$$

$$Mn_3O_4 + 4\,CO_2 + C_8H_{18} \longrightarrow Mn_3O_4 + C_8H_{18} + 4\,CO_2 + \uparrow$$

$$Mn_3O_4 + C_8H_{18} \longrightarrow C_8H_{18}\uparrow$$

$$Mn_3O_4 \longrightarrow 3\,MnO + 1/2\ O_2\uparrow$$

3.5 Optical Properties: UV - Visible Spectroscopy

UV-Visible spectroscopy was employed to investigate the optical properties of the biosynthesized manganese oxide (MnO_2) nanostructures. The absorbance behaviour is influenced by several factors, including impurity centers, surface roughness, oxygen vacancies, and band gap energy.

Figure 6 illustrates the UV-Vis absorption spectrum of MnO_2 nanoparticles recorded at room temperature. A distinct absorption peak is observed at 365 nm, which corresponds to the electronic transition characteristic of MnO_2 nanostructures. This absorption is indicative of the formation of well-defined nanoscale manganese oxide particles.

The optical band gap of the synthesized MnO_2 nanoparticles was estimated using the Tauc plot method and found to be approximately 3.39 eV. This wide band gap suggests that the nanomaterial is semiconducting in nature and possesses strong potential as an efficient photo catalyst in environmental remediation and other photocatalytic applications.

4. Photocatalytic Activity of MnO_2 Nanoparticles

The photocatalytic performance of the synthesized MnO_2 nanoparticles was evaluated through the degradation of two organic dyes methyl orange (MO) and bromocresol green (BCG) under natural sunlight irradiation. In each experiment, approximately 10 mg of MnO_2 NPs was added to a solution containing 10 mL of dye (25 mg/L concentration) and 1 mL of $NaBH_4$ solution (3×10^{-2} mol/L). The reaction mixtures were placed in screw-cap vials, thoroughly mixed, and then exposed to direct solar radiation. UV–Visible spectra were recorded at regular intervals over a period of 60 minutes to monitor the extent of decolourization.

The catalytic efficiency of MnO_2 NPs in degrading MO and BCG is illustrated in Fig. 8. A noticeable decrease in the absorption intensity of the dyes was observed, indicating significant photocatalytic degradation. The efficiency of degradation was calculated using the equation:

$$colour\ removal\ (\%) = \ (C_0 - \ \backslash raisebox1ex\$C_t\$/\backslash raisebox-1ex\$C_0\$)\ x\ 100$$

where C_0 (mg/L) and C_t (mg/L) represent the dye concentrations at time zero and time *t*, respectively.

After 60 minutes of irradiation, the MnO_2 NPs demonstrated a high photocatalytic activity, achieving approximately 90% decolourization of methyl orange and 93% of bromocresol green at neutral pH. These results confirm the efficiency of the biosynthesized MnO_2 nanoparticles as effective photo catalysts.

The photocatalytic degradation mechanism involves the excitation of electrons from the valence band (VB) to the conduction band (CB) upon absorption of photons with energy equal to or greater than the band gap energy (E_g). This excitation results in the formation of electron-hole pairs. These charge carriers migrate to the nanoparticle surface, where they interact with molecular oxygen (O_2) and water (H_2O) to generate reactive oxygen species (ROS), including hydroxyl (•OH) and superoxide (O_2^{-}•) radicals, which contribute to the degradation of dye molecules.

Kinetic analysis of the photocatalytic degradation was carried out by plotting $\ln(A_0/At)$ versus time (Figs. 8 and 10). The linear relationship indicates that the degradation follows a pseudo-first-order reaction model. The rate constants (*k*) for MO and BCG degradation were calculated to be 0.020 min^{-1} and 0.026 min^{-1}, respectively.

Additionally, the degradation of dyes with $NaBH_4$ in the absence of MnO_2-NPs was also examined. Although $NaBH_4$ is a known reducing agent and thermodynamically favourable for breaking azo bonds in MO and BCG to form amino derivatives, the reaction proceeded very slowly due to kinetic limitations. In contrast, the presence of MnO_2 NPs provided an alternative reaction pathway with a lower activation energy, thereby enhancing both the thermodynamic and kinetic feasibility of dye degradation.

These findings suggest that biosynthesized MnO_2 nanoparticles possess excellent photocatalytic capabilities and are promising candidates for environmental applications such as wastewater treatment.

4.1 Methyl Orange (MO):

4.2 Bromocresol green (BCG)

5. Conclusions

In this study, manganese dioxide (MnO_2) nanoparticles were successfully synthesized via a green synthesis route using *Lagerstroemia speciosa* leaf extract as a natural reducing and stabilizing agent. The X-ray diffraction (XRD) analysis confirmed that the synthesized nanoparticles exhibit a polycrystalline tetragonal phase with an average crystallite size of 25.3 nm, as calculated using Scherrer's equation. Field Emission Scanning Electron Microscopy (FESEM) revealed that the MnO_2 nanoparticles possess irregular, aggregated, and roughly spherical morphologies, with particle sizes ranging from 83 nm to 400 nm. The observed aggregation is attributed to the high surface energy and polarity of the nanoparticles, along with electrostatic interactions. These morphological features contribute to an increased surface area, which enhances the adsorption efficiency of the nanoparticles for dye degradation.

The UV visible spectroscopy results showed a strong absorption peak at 365 nm, corresponding to the MnO_2 nanostructures, with a calculated optical band gap of 3.39 eV, indicating their potential for visible-light-driven photo catalysis. Photocatalytic degradation experiments demonstrated that the MnO_2 nanoparticles efficiently degraded both methyl orange and bromocresol green dyes within 60 minutes, achieving near-complete decolourization. The reduction in absorbance at 460 nm further confirms the complete degradation of the dye molecules.

Overall, the biosynthesized MnO_2 nanoparticles exhibit promising structural, optical, and photocatalytic properties, highlighting their potential for application in environmental remediation, particularly in the treatment of dye-contaminated wastewater.

Declarations

Competing Interest

The authors declare no competing interest.

Funding Statement:

The authors declare that no funds, grants, or other support were received during the preparation of this manuscript.

Author Contribution

Jagdish Arekar: Conceptualization, methodology, investigation, data curation, writing original draft preparation.Dipak Garole: Formal analysis, supervision, writing review and editing.R. S. Bendre: Resources, validation, project administration, supervision, funding acquisition.Yogesh R. Toda: Visualization, writing original draft preparation, software support, data curation, writing review and editing.All authors have read and approved the final version of the manuscript.

Acknowledgement

The authors gratefully acknowledge the lab personnel of thin film laboratory, Pratap College, Amalner, School of Chemical Sciences, K.B.C. North Maharashtra University, Jalgaon and Directorate of Geology and Mining, Government of Maharashtra, Nagpur for their generous support during the research work.

References

1. Dr. G. Sakthi, and Dr. P. Saravanakumari, Green Synthesis of Manganese Oxide Nanoparticles using *Phyllanthusacidus*, International J. of Multidisciplinary Educational Research, Vol. 10 Issue 4 (7) (April 2021) 112–116.
2. Siddique M, Fayaz N, Saeed M, Synthesis, characterization, photocatalytic activity and gas sensing properties of zinc doped manganese oxide nanoparticles. Phys. Rev. B. Condens. Matter 602 (2021) 412504. https://doi.org/10.1016/j. physb. 2020.412504.
3. M. Jayandran, M. MuhamedHaneefa, V. Balasubramanian, Green synthesis and characterization of Manganese nanoparticles using natural plant extracts and its evaluation of antimicrobial activity, Journal of Applied Pharmaceutical Science Vol. 5 (12) (December, 2015) 105–110, DOI: 10.7324/JAPS.2015.501218.
4. Chen HJ, Tian W, Ding W. Effect of preparation methods of the morphology of active manganese dioxide and 2, 4Dinitrophenol adsorption performance; Adsorption Science And Technology 36 (3–4) (2018) 1100–1111. DOI: 10.4172/2169-0022.1000172.
5. Sagadevan S. Investigations synthesis, structural, morphological and dielectric properties of manganese oxides nanoparticles; Journal of Material Sciences & Engineering. 4(3) (2015) 1–3.
6. Feng L, Xuan Z, Zhao H, Bai Y, Guo J, Su CW, MnO prepared by hydrothermal method and electrochemical performance as anode for lithium-ion battery. Nanoscale Research Letters, 9 (290) (2014) 1–8.
7. S. Mitra, Y. Pak, N. Alaal, M.N. Hedhili, D.R. Almalawi, N. Alwadai, K. Loganathan, Y. Kumarasan, N. Lim, G.Y. Jung, I.S. Roqan, Novel P-Type Wide Band Gap Manganese Oxide Quantum Dots Operating at Deep UV Range for Optoelectronic Devices, Adv. Opt. Mater. 7 (21) (2019) 1900801
8. M. M. Najafpour, S. I. Allakhverdiev, Manganese compounds as water oxidizing catalysts for hydrogen production via water splitting: From manganese complexes to nano-sized manganese oxides, Int. J. Hydrogen Energy 37 (2012) 8753–8764, https://doi.org/10.1016/J.IJHYDENE.2012.02.075.

9. H.T. Zhang, X.H. Chen, J.H. Zhang, G.Y. Wang, S.Y. Zhang, Y.Z. Long, Z.J. Chen, N. L. Wang, Synthesis and characterization of one-dimensional $K_{0.27}MnO_2$-0.5H_2O, J. Cryst. Growth 280 (1–2) (2005) 292–299.
10. Q. Shu-yan, F. Jing, Y. Jun, Hydrothermal synthesis and super capacitor properties of urchin sphere and nanowire MnO_2, Chinese J. Nonferrous Met. 18 (2008) 113–117.
11. Haibin Lu, Xueyang Zhang, Ahmad Khan, Wenqiang Li, Lei Wan, Biogenic Synthesis of MnO2 Nanoparticles with Leaf Extract of *Voila betonicifolia*for Enhanced Antioxidant, Antimicrobial, Cytotoxic and Biocompatible Applications, Frontiers in Microbiology, 12 (Nov. 2021) 761084; doi: 10.3389/fmicb.2021.761084
12. K. S. Shaker, A. H. Abdalsalm, Characterization Nano Structure of MnO_2 via Chemical Method, Eng Technol. J. 36 (2018) 946–950.10.30684/etj.36.9A.1
13. Sanjay S. Majani, SreelakshmiSathyan, MeghaVadakkethil, Manoj, Nimisha Vinod, Sushma Pradeep, Chandan Shivamallu, Venkatachalaiah K. N, Shiva Prasad Kollur, Eco-friendly synthesis of MnO nanoparticles using *Saracaasoca* leaf extract and evaluation of *in vitro* anticancer activity, Current Research in Green Sustainable Chemistry, 6 (2023) http://doi.org/10.1016/j.crgsc.2023.100367
14. A.Cauerhff, G. R. Castro, Bio-nanoparticles, a green nano - chemistry approach, Electronic Journal of Biotechnology, Review 16 (3) (2013) 1–10. Available: www.ejbiotechnology.info DOI: 10.2225.
15. A. G. Ingale, A. N. Chaudhari, Biogenic synthesis of nanoparticles and potential applications: an eco-friendly approach, Journal of Nanomedicene and Nanotechnology, 2 (2013) 1–7. DOI: 10. 4172/2157-7439.1000165.
16. Ibrahim Mohamed Abouzeid Hasan, Hassan M. A. Salman, Olfat M. Hafez, Ficus-mediated green synthesis of manganese oxide nanoparticles for adsorptive removal of malachite green from surface water, Environmental Science and Pollution Research, 30 (2023) 28144–28161, https://doi.org/10.1007/s11356-022-24199-8
17. AKM Atique Ullah, Md. Mahbubul Haque, MahmudaAkter, AHossain, Md. Mottaleb Hosen, AKM Fazle Kibria, MNI Khan and MKA Khan, Green synthesis of Bryophyllumpinnatum aqueous leaf extract mediated bio-molecule capped dilute ferromagnetic α-MnO_2 nanoparticles, Mater. Res. Express 7 (2020) 015088, DOI: 10.1088/2053-1591/ab6c20.
18. Madhumitha G, Fowsiya J, Gupta N, Kumar A, Singh M, Green synthesis, characterization and antifungal and photocatalytic activity of Pithecellobium dulce peel mediated ZnO nanoparticles, J Phys. Chem. Solids 127 (2019) 43–51, https://doi.org/10.1016/j.jpcs.2018.12.005
19. Ibrahim Mohamed Abouzeid Hasan, Hassan M. A. Salman, Olfat M. Hafez, Ficus-mediated green synthesis of manganese oxide nanoparticles for adsorptive removal of malachite green from surface water, Environmental Science and Pollution Research 30 (2023) 28144–2816, https://doi.org/10.1007/s11356-022-24199-8
20. Y. Dessie, S. Tadesse, R. Eswaramoorthy, Physicochemical parameter influences and their optimization on the biosynthesis of MnO_2 nanoparticles using Vernonia amygdalina leaf extract, Arab J Chem. 13 (2020) 6472–6492. https://doi.org/10. 1016/j. arabjc.2020. 06. 006.

21. S. Karnchanawong and P. Limpiteeprakan, Evaluation of Heavy Metal Leaching from Spent Household Batteries Disposed in Municipal Solid Waste, Waste Management, Vol. 29, No. 2 (2009) 550–558. doi:10.1016/j.wasman.2008.03.018.
22. Susana M Xará, Julanda N Delgado, Manuel Almeida, Carlos A. V. Costa, Laboratory study on the leaching potential of spent alkaline batteries, Waste Management 29(7) (April- 2009) 2121–31, DOI: 10.1016/j.wasman.2009.03.010.
23. M Mylarappa, V Venkata Lakshmi, K R Vishnu Mahesh, H P Nagaswarupa, N Raghavendra; A facile hydrothermal recovery of nano sealed MnO_2 particle from waste batteries: An advanced material for electrochemical and environmental applications, IOP Conf. Series: Materials Science and Engineering 149 (2016) 012178, doi:10.1088/1757-899X/149/1/012178.
24. Jannatun Zia, Elham Aazam, Ufana Riaz, Synthesis of nanohybrids of polycarbazole with α-MnO2 derived from Brassica oleracea: a comparison of photocatalytic degradation of an antibiotic drug under microwave and UV irradiation, Environmental Science and Pollution Research 27(19) (July 2020) 24173–24189, https://doi.org/10.1007/s11356-020-08149.w.
25. Vahid Hoseinpour, MahsaSouri, Nasser Ghaemi, Green synthesis, characterisation, and photocatalytic activity of manganese dioxide nanoparticles, Micro & Nano Letters, 13, Iss. 11 (2018) 1560–1563; doi:10.1049/mnl.2018.5008
26. Kollur Shiva Prasad and Alakananda Patra, Green synthesis of MnO_2 nanorods using Phyllanthus amarus plant extract and their fluorescence studies, Green Processing and Synthesis, 6 (2017) 549–554; https://doi.org/10.1515/gps-2016-0166
27. Mamun M A A, Noor M, Ullah A K M A, Hossain M S, Matin M A, Islam F and Hakim M A, Effect of $CePO_4$ on structural, magnetic and optical properties of ceria nanoparticles, Mater. Res. Express 6 (1) (2018) 016102, DOI 10.1088/2053 – 1591/aae2d0.
28. A. Bystrom and A. M. Bystrom, The crystal structure of hollandite, the related manganese oxide minerals, and α-MnO2, Acta Cryst. 3 (1950) 146–54, https://doi.org/10.1107/S0365110X5000032X.
29. Mariya Moeen, Shazia Nouren, Maria Zaib, Ismat Bibi, Abida Kausar&Misbah Sultan, Green synthesis, characterization and sorption efficiency of MnO_2 nanoparticles and MnO_2@waste eggshell nanocomposite, Journal of Taibah University for Science, 16 No. 1 (2022) 1075–1095; https://doi.org/10.1080/16583655.2022.2139483
30. A. Martin Joseph and R. Thilak Kumar, Formation and investigation of low dimensional super paramagnetic α-manganese dioxide nanostructures, Materials Research Express, Vol. 5 No. 1(Jan. 2018); DOI: http://dx.doi.org/10.1088/2053-1591/aa9e5d
31. YuXin Zhang, Shijin Zhu, Meng Dong, Chuan Pu Liu, Zhong Quan Wen, Hydrothermally Tailoring Low-dimensional MnO_x Nanostructure and Their High Electrochemical Performance, International Journal of Electrochemical Science, Vol. 8, Issue 2 (Feb 2013) 2407–2416; https://doi.org/10.1016/S1452-3981(23)14318-5

Figures

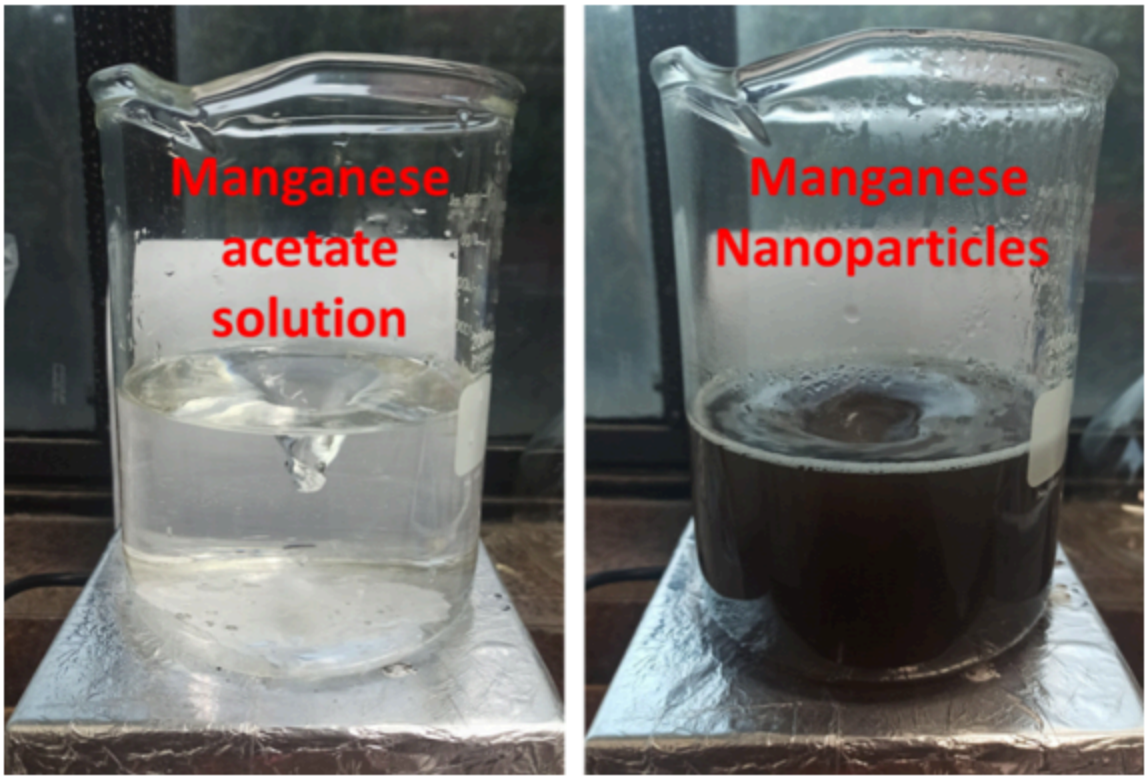

Figure 1

Formation of manganese oxide nanoparticles (MnO_2-NPs) during the synthesis process.

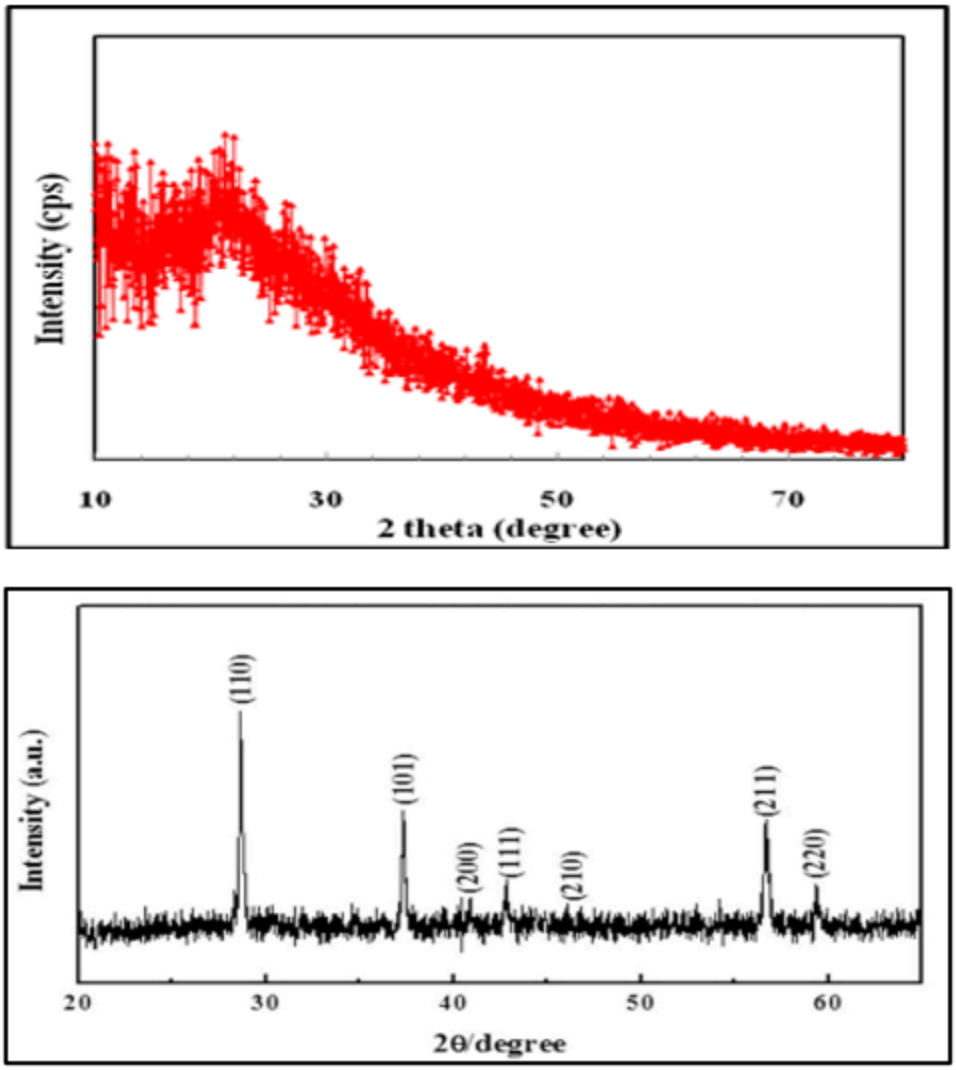

Figure 2

XRD- Diffractograms of Manganese Oxide Nanoparticles

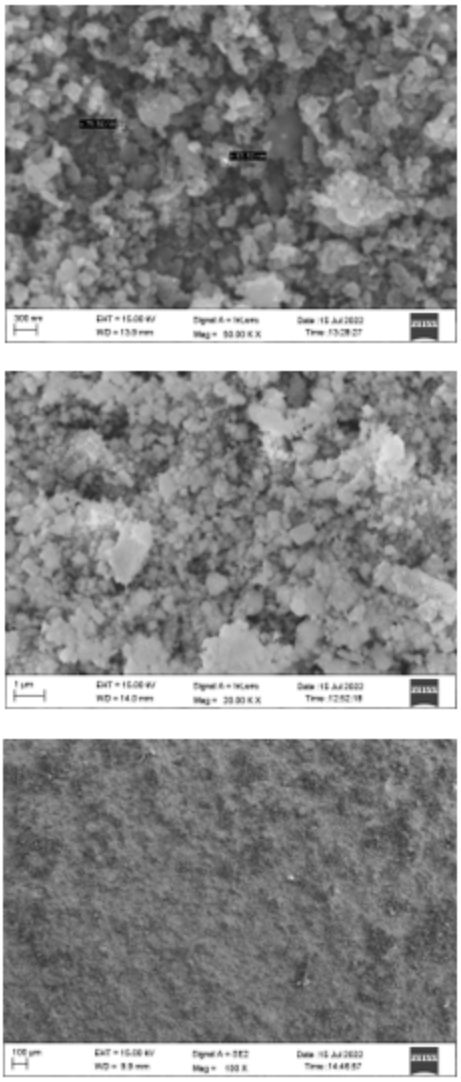

Figure 3

(a to c):FE-SEM Images of Manganese Nanoparticles.

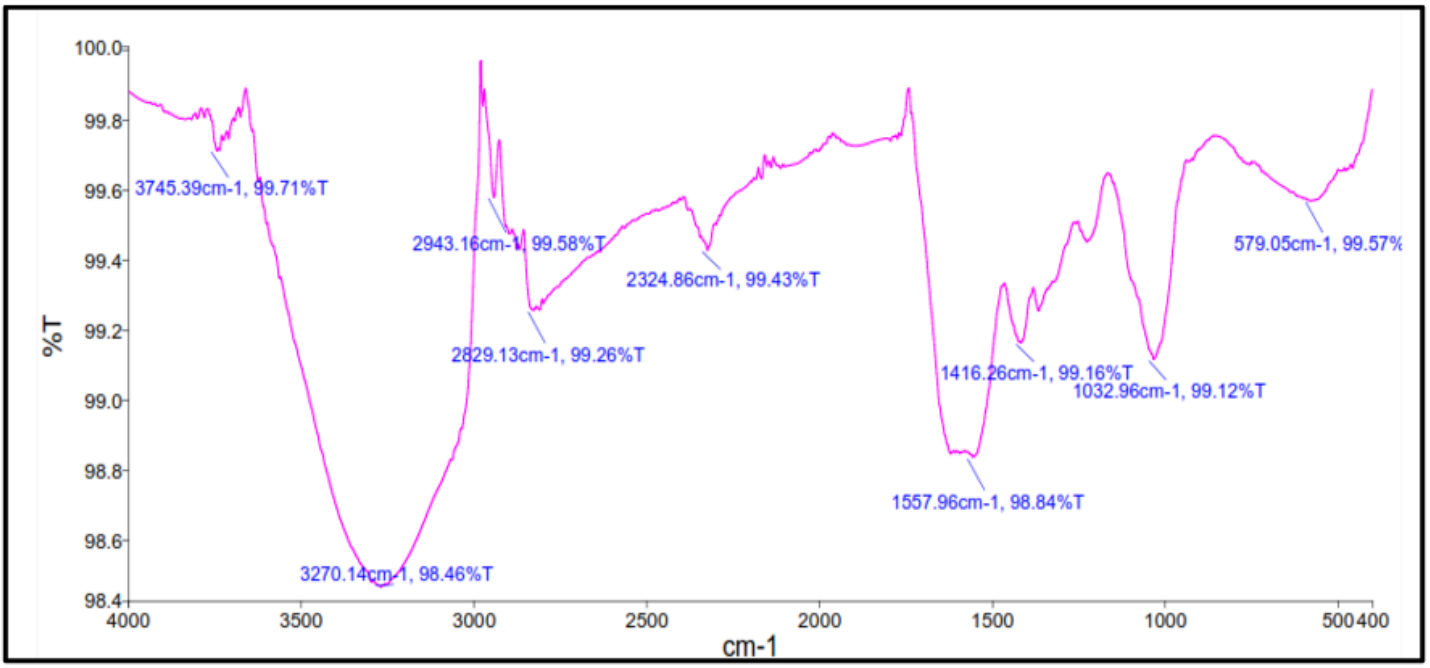

Figure 4

FTIR spectrum of Manganese oxide Nanoparticles

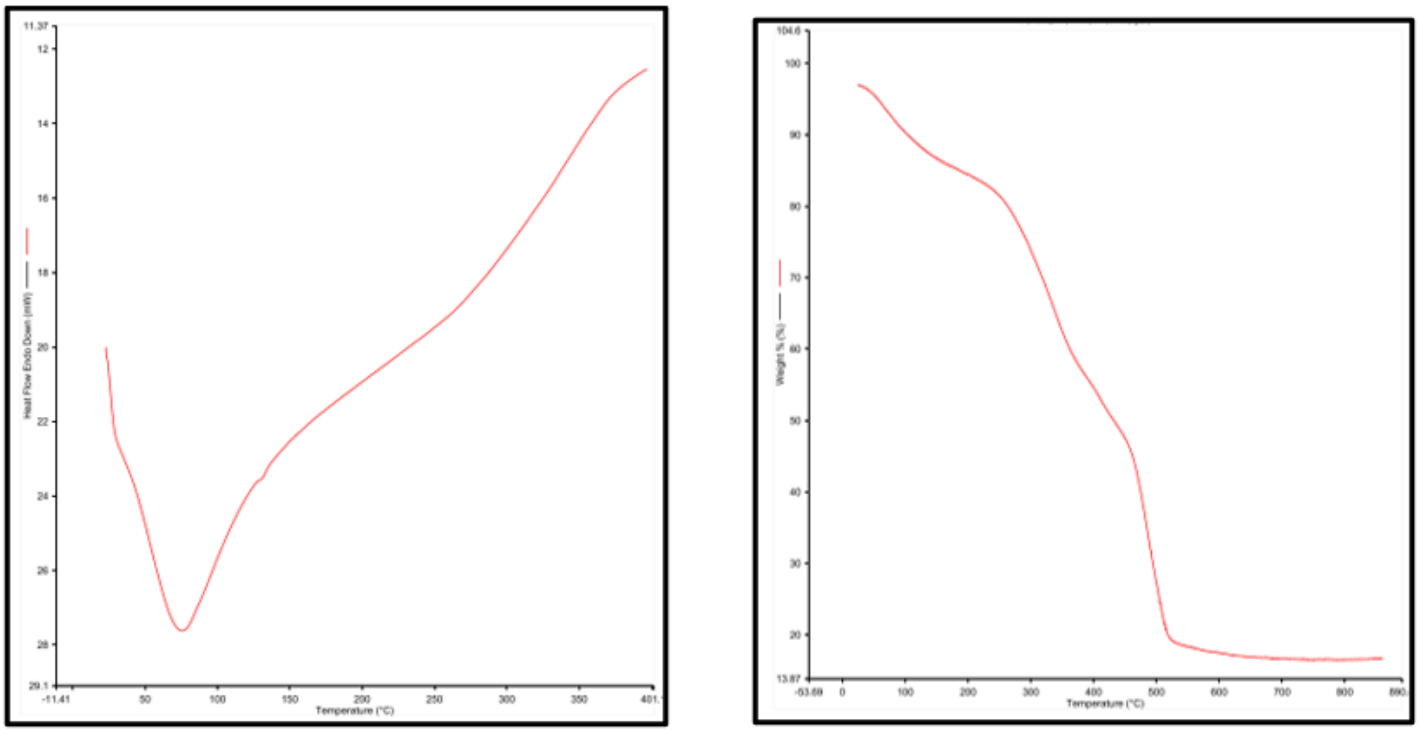

Figure 5

(a to b): TGA/DTA curves of the Manganese Oxide Nanoparticles

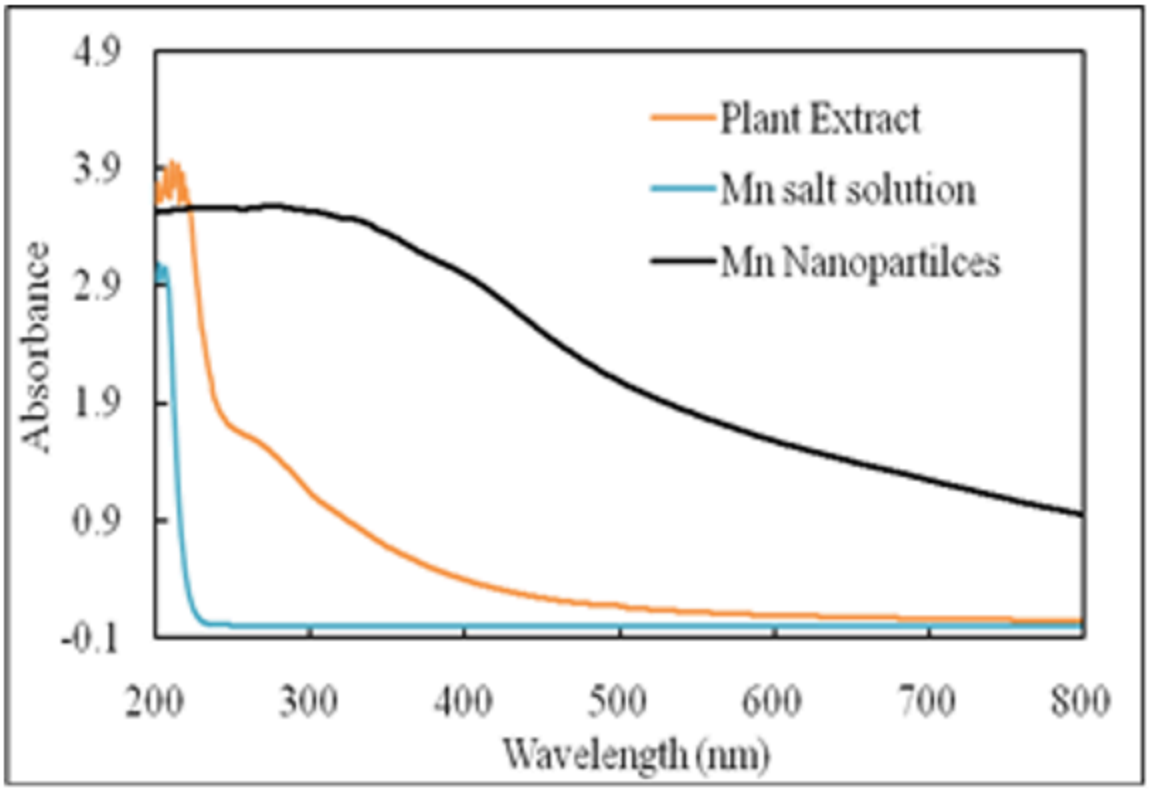

Figure 6

UV-Vis spectra of plant extract, Mn solution, and biosynthesized Mn nanoparticles

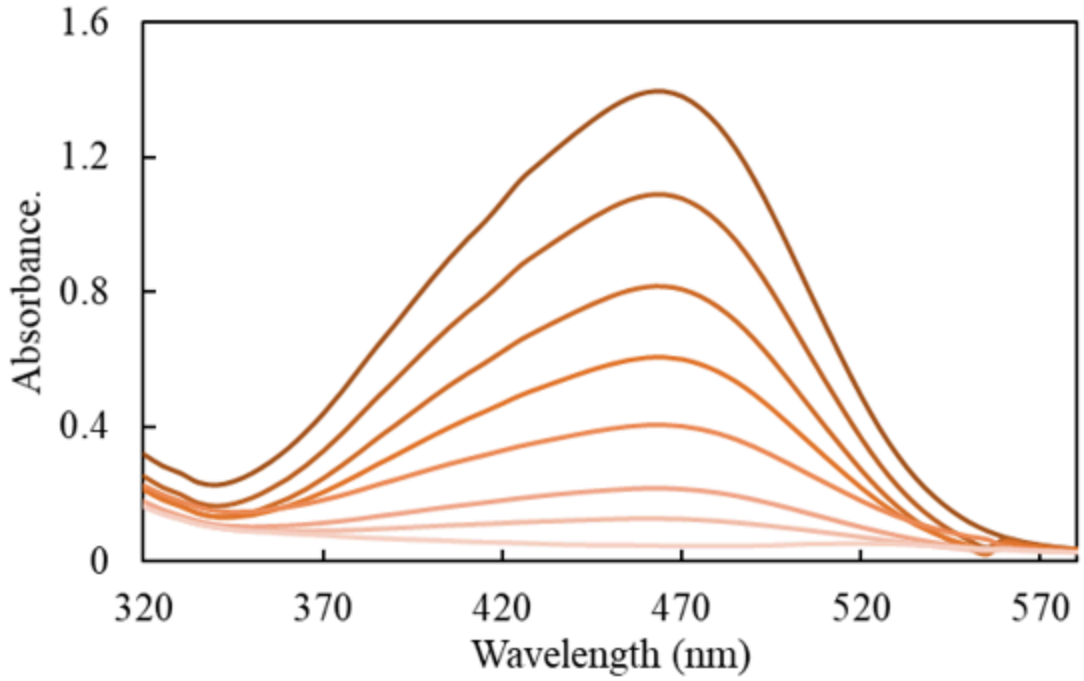

Figure 7

UV-Visible Absorbance Spectrum of Methyl Orange & MnO_2 NPs Reaction Mixture

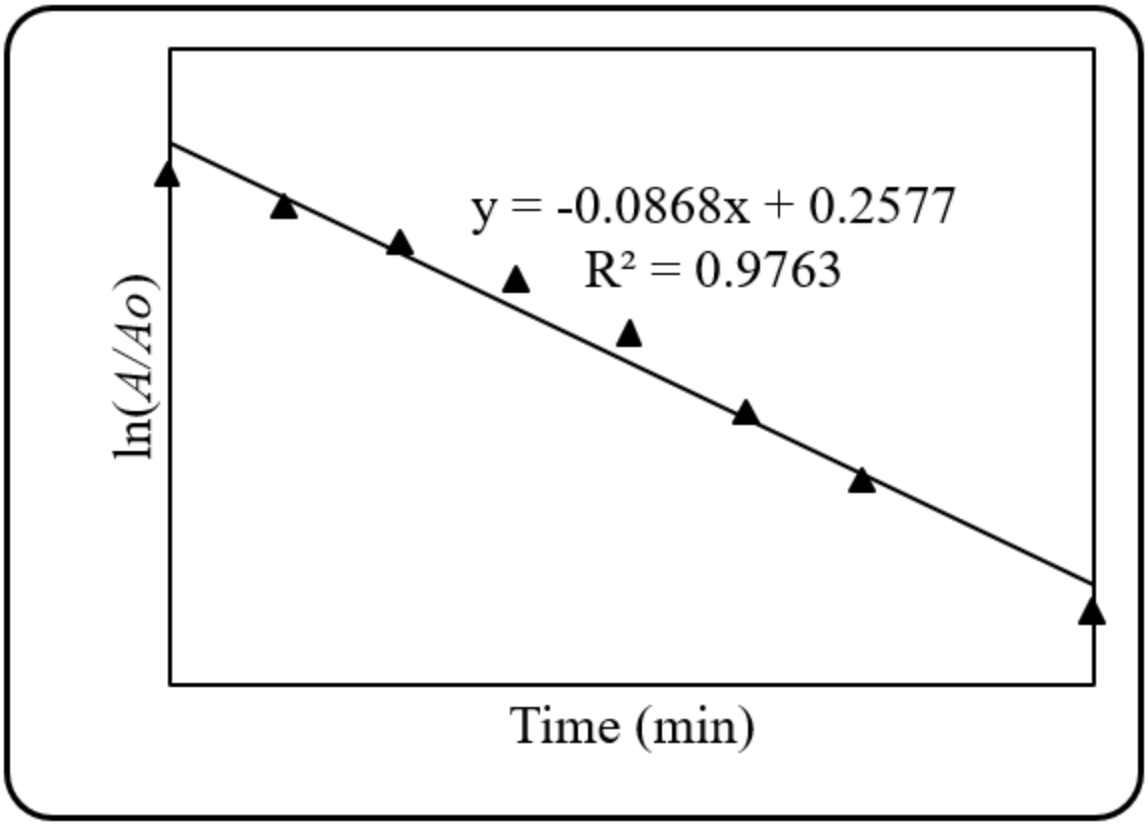

Figure 8

Calibration Curve [Ln (At/Ao) vs. time

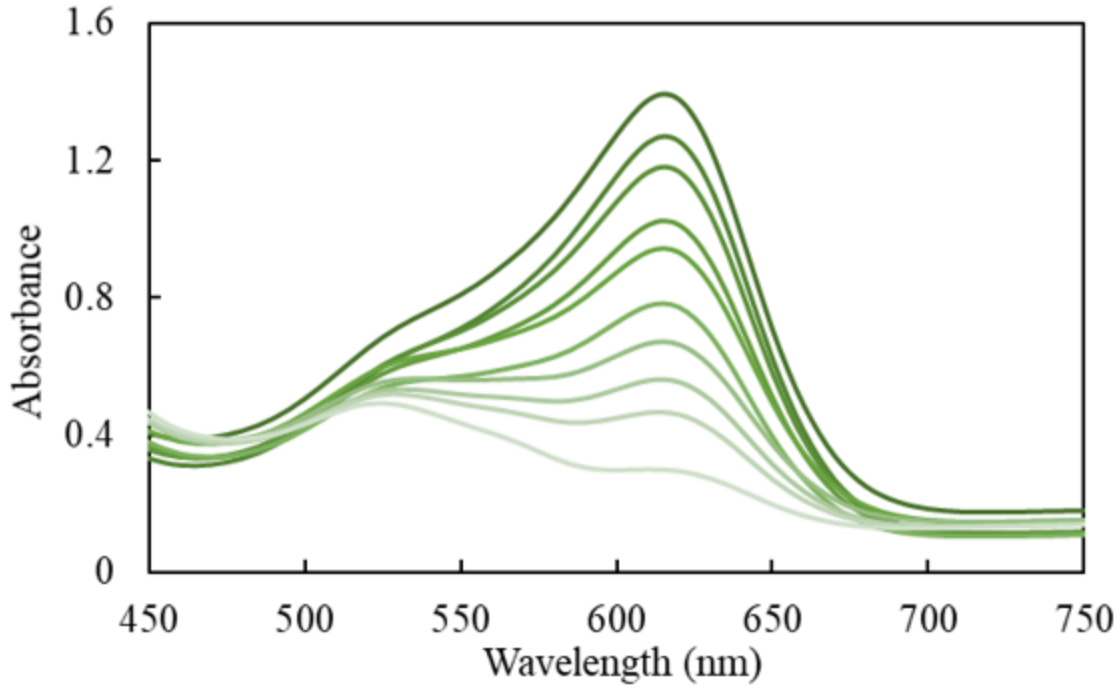

Figure 9

UV-Visible Absorbance Spectrum of Bromocresol Green & MnO_2 NPs Reaction Mixture

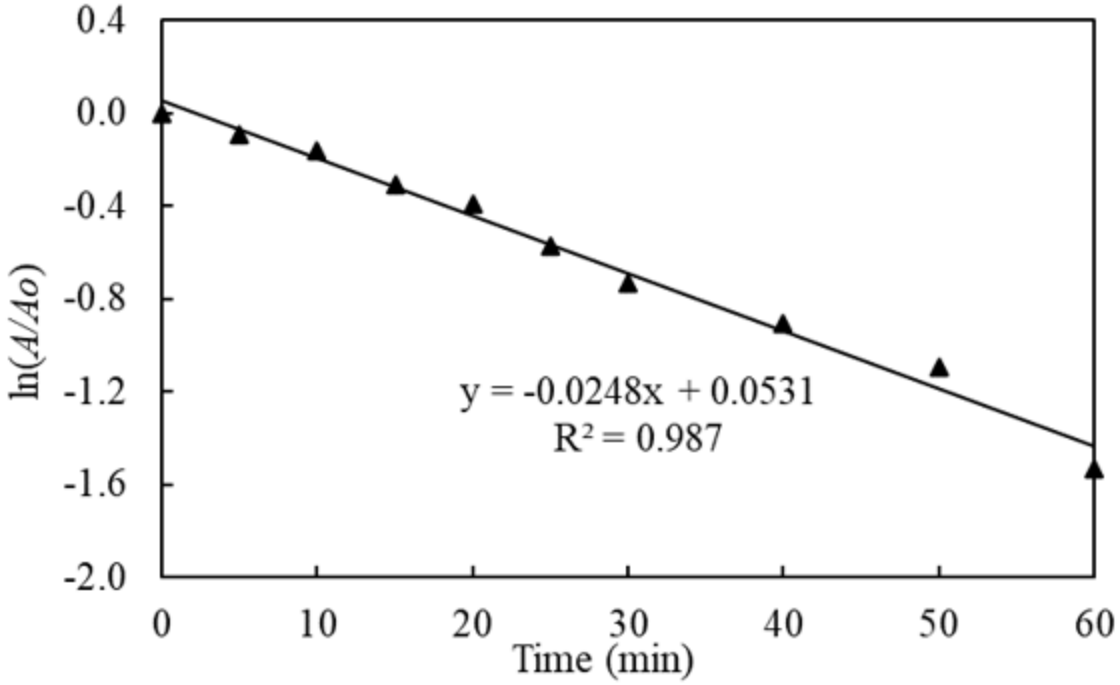

Figure 10

Calibration Curve [Ln (At/Ao) vs. time

Supplementary Files

This is a list of supplementary files associated with this preprint. Click to download.

- TEATGA.pdf
- GA.png